A DESIGN AND CHARACTERISTICS OF SWITCHED RELUCTANCE TYPE BEARINGLESS MOTORS

Masatsuga Takemoto, Ken Shimada, Akira Chiba
Chiba Laboratory, Department of Electrical Engineering
Faculty of Science and Technology,
Science University of Tokyo

Tadashi Fukao
Tokyo Institute of Technology

SUMMARY

Switched reluctance type bearingless motors have been proposed. The principle of radial force generation is explained on a stator with differential winding configurations. The radial force is a function of the radial force winding current and the motor current, as well as the rotor rotational position. If salient poles are unaligned, the radial force is the minimum. In this condition, fringing fluxes play an important role. In this paper, the theoretical equations of radial forces are derived with a close examination of the flux distribution. Based on results of FEM analysis, a simple mathematical equation is proposed to express fringing fluxes neglecting magnetic saturation. The radial force and current relationships are derived with the fringing effects. The derived equations are found to be effective especially at unaligned positions.

I. INTRODUCTION

Recently, various bearingless motors have been proposed, for example, reluctance [1], induction [2-4], permanent magnet [5-6], etc. These motors each have nice characteristics of their own. Recently, there has been interest in switched reluctance motors. For very special environments, switched reluctance motors have superior possibilities, because switched reluctance motors have several advantages such as fail safe, rotor robustness, low cost and possible operation in high temperatures or at high rotational speeds [7-8].

Moreover, switched reluctance motors have nice possibilities as bearingless motors. In principle, torque is generated by magnetic attraction of rotor and stator poles. In this process, significant amounts of radial force are generated. Thus, in practice, switched reluctance motors are famous for noises and vibration because fairly high radial force is exerted in the air-gaps. It is very possible to take advantage of these high radial forces for bearingless motors.

Switched reluctance motors have a stator with concentric windings around salient poles. Thus, if currents in the concentric windings of each pole are controlled independently, both radial force and torque can be controlled. To the author's best knowledge, this idea was originally proposed by Prof. Higuchi [9] in 1989. The same idea can also be seen in [10]. The ideas are good for only low rotational speed motors such as torque drives and positioning drives. In the case of power conversion, rotational speeds are high so that motor back E.M.F. is high. Thus, it is unavoidable to increase the voltage ratings of drive inverters to have fast control of radial forces. In practice, voltage and current ratings of drive inverters should be minimized to be cost competitive. Then, instantaneous current control is difficult at high rotational speeds. The current control can be fast enough for torque control; however, it cannot be fast enough for radial force control required in magnetic suspension.

Professor Higuchi also proposed a stepping motor with magnetic suspension windings [11]. His idea took advantage of the multi-pole per stator tooth configuration in variable reluctance motors. Radial force is not influenced by motor current due to having several poles for a stator tooth. This motor is good for positioning drives as he proposed, however, not for power conversion because of many poles, high inductance as well as high leakage fluxes. For power conversions, switched reluctance motors have stator and rotor combinations of 12/8, 8/6, or 6/4, with only one pole for a tooth.

It is important to apply recent ideas of differential windings of bearingless motors to switched reluctance motors to be practical and reduce voltage and current required for magnetic suspension. A stator winding configuration with differential windings for switched reluctance motors with one pole for a stator tooth has been proposed by the authors [12]. Principles of radial force production were explained. The relationships between radial force and current were found to be dependent to rotor rotational positions unlike Prof. Higuchi's [11]. If rotor and stator poles are aligned, radial force is effectively produced. However, radial force is low at unaligned positions. For successful magnetic suspension, radial force must be controlled at any rotational position. Successful control can then be realized by integrated digital controllers. Thus, analysis of unaligned positions is very important.

In this paper, effects of fringing fluxes are examined using FEM analysis. Then, a simple mathematical equation is proposed for further analysis. Relationships between radial force and current around unaligned positions are derived. These relationships are confirmed in experiments.

II. PRINCIPLES OF PROPOSED MACHINES

A. Configuration of a stator core and windings

Fig. 1 shows a cross section of stator and rotor cores on a prototype machine. The iron cores of a stator and a rotor are made up of laminated silicon steel which is simply stamped out to salient pole form. The laminated silicon steel has a thickness of 0.35mm. The stack length is 50mm. It is noted that the stator has 12 poles and the rotor has 8 poles.

Fig. 2 shows the A-phase winding configuration. The motor winding current i_{ma} flows into four coils connected in series. One coil is three paralleled wires having a diameter of 0.8mm and 14 turns in series. On the other hand, radial force winding currents i_{sa1} and i_{sa2} flow into two coils, respectively. These coils are separately wound around each stator tooth. These coils are two paralleled wires having a diameter of 0.8mm and 11 turns in series. The B-phase winding configuration is situated on one third rotational position of the A-phase. The C-phase winding configuration is situated on two thirds rotational position of the A-phase. The axes a_1 and a_2 of a perpendicular coordinate can be defined based on the A-phase winding configuration. In this case, the axes α and β are aligned with a_1 and a_2, respectively. In addition, the axes of coordinates b_1, b_2, c_1 and c_2 can be defined based on the B- and C-phase windings, respectively.

B. Principles of radial force generation

Fig. 3 shows the principles of radial force production of the proposed bearingless motors. Stator teeth and rotor teeth of this figure are situated in the aligned position. The symmetrical 4-pole fluxes are produced from the 4-pole motor winding current i_{ma}. These thick solid lines show the instantaneous flux direction of the 4-pole magnetic field at a certain moment. The symmetrical 2-pole fluxes are also generated from 2-pole radial force winding current i_{sa1}. These broken lines show the instantaneous flux direction of the 2-pole magnetic field for radial position control.

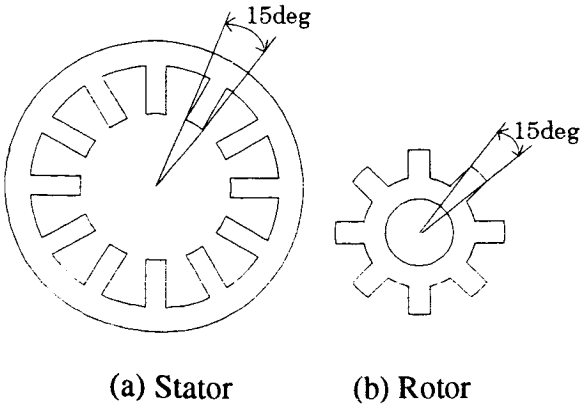

(a) Stator (b) Rotor

Fig. 1 Cross section of a prototype machine.

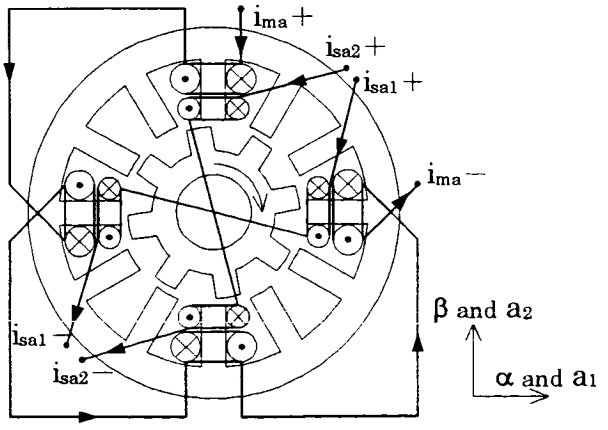

Fig. 2 A-phase winding configuration.

The rotor radial position control with a negative feedback loop can be explained as follows. If the rotor moves toward the negative direction in the α-axis from the stator center, the flux distribution in the air-gap is unbalanced. A radial force toward the negative direction in the α-axis is generated. In order to balance with this force, a positive current i_{sa1} is fed in the 2-pole radial force winding, which produces the 2-pole fluxes as shown in Fig. 3. Therefore, the flux density in the air-gap 1 is increased, because the direction of the 2-pole fluxes is the same as that of the 4-pole fluxes. On the contrary, the flux density in the air-gap 2 is decreased, as the direction of the 2-pole fluxes is opposite to that of the 4-pole fluxes. This superimposed magnetic field results in the radial electromagnetic force F acting to the rotor in the α-direction.

On the other hand, a radial force opposite to the α-direction can be produced with a negative current i_{sa1} in the 2-pole radial force winding. Moreover, a radial force in β-direction can be produced by 2-pole radial force winding current i_{sa2}. Thus, radial force can be produced in any desired direction.

The above is the case of A-phase, in the same way, this principle can be applied to the B- and C-phase. The direction of a radial force on the B- and C-phase differs from that on the A-phase. Therefore, transformation of coordinates is required. In switched reluctance motors, all three phases are not excited at one moment. Rather, only one out of three phases is excited at a low speed. If at least one of three phases is excited, the radial force can be produced in any desired direction with the proposed winding configuration. It is noted that the air-gap flux density depends on the rotor rotational position. The stator and rotor poles are aligned in Fig. 3. High radial force can be produced in this condition, however, radial force is reduced at unaligned positions. At unaligned positions, fringing fluxes play an important role.

III. DERIVATION OF INDUCTANCES

A. Magnetic equivalent circuit

Fig. 4 shows a cross section of a prototype machine superimposed by a magnetic equivalent circuit and each phase winding configuration. Voltage sources show magnetomotive forces (MMFs) of the 4-pole motor windings and the 2-pole radial force windings, in addition, permeances of air-gaps are expressed as resistances.

Fig. 5 shows a magnetic equivalent circuit only for the A-phase, which is extracted from Fig. 4. The definitions of Fig. 5 are as follows:

N_m number of turns of the motor winding.
N_b number of turns of the radial force winding.
i_{ma} an instantaneous current of the motor winding.
i_{sa1} an instantaneous current of the radial force winding on the a_1-axis.
i_{sa2} an instantaneous current of the radial force winding on the a_2-axis.
P_{a1}~P_{a4} permeances of air-gaps at A-phase winding poles.
ϕ_{a1}~ ϕ_{a4} magnetic fluxes of each tooth.

Only A-phase magnetic equivalent circuit is used to have a simple calculation in this paper. This is possible because switched reluctance motors have little mutual inductance among the A-, B-, and C-phases.

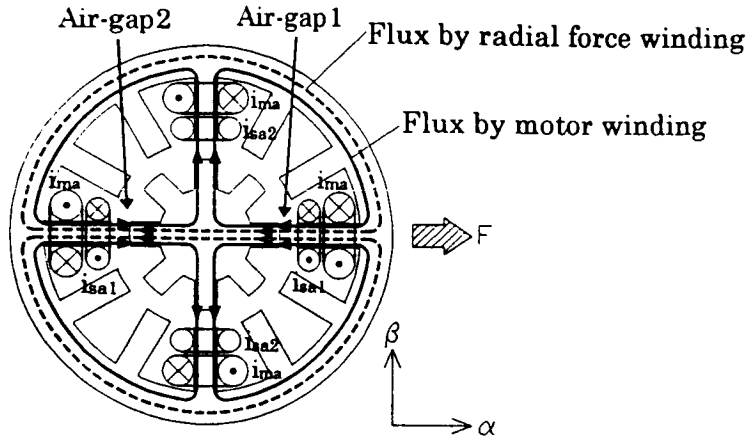

Fig.3 Principle of radial force generation.

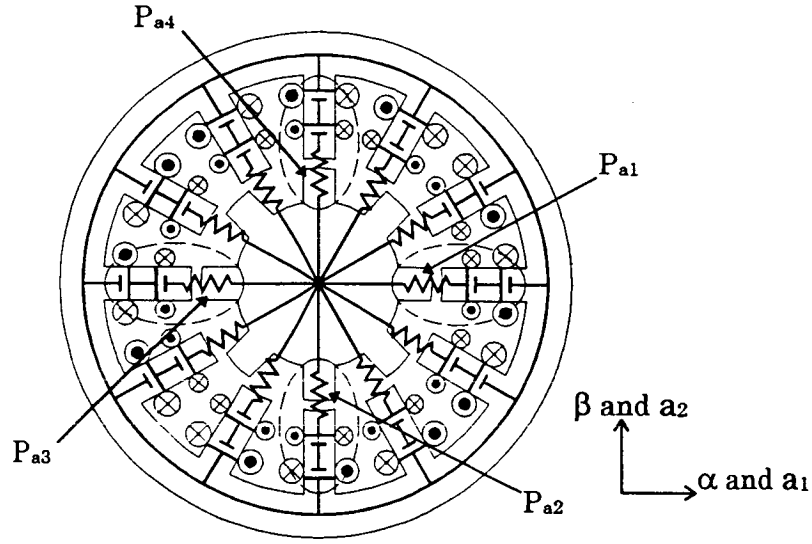

Thick solid lines : Magnetic equivalent circuit.
Broken lines : M.M.F. and permeance of A-phase.

Fig.4 Winding configuration and a magnetic equivalent circuit.

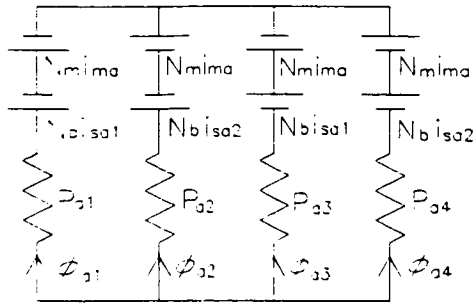

Fig.5 A magnetic equivalent circuit of A-phase.

The following equations (1)~(3) are given from Fig. 5, because a sum of the magnetomotive forces in each branch is equal to another one.

$$\frac{\phi_{a2}}{P_{a2}} - N_m i_{ma} + N_b i_{sa2} = \frac{\phi_{a1}}{P_{a1}} + N_m i_{ma} + N_b i_{sa1} \tag{1}$$

$$\frac{\phi_{a3}}{P_{a3}} + N_m i_{ma} - N_b i_{sa1} = \frac{\phi_{a1}}{P_{a1}} + N_m i_{ma} + N_b i_{sa1} \tag{2}$$

$$\frac{\phi_{a4}}{P_{a4}} - N_m i_{ma} - N_b i_{sa2} = \frac{\phi_{a1}}{P_{a1}} + N_m i_{ma} + N_b i_{sa1}. \tag{3}$$

Because a sum of the magnetic fluxes is equal to zero, it can be written as,

$$\phi_{a1} + \phi_{a2} + \phi_{a3} + \phi_{a4} = 0. \tag{4}$$

ϕ_{a1}~ϕ_{a4} can be derived from the equations (1)~(4) as,

$$\phi_{a1} = \frac{-P_{a1}}{P}\left[2N_m(P_{a2}+P_{a4})i_{ma} + N_b(P_{a2}+2P_{a3}+P_{a4})i_{sa1} - N_b(P_{a2}-P_{a4})i_{sa2}\right] \tag{5}$$

$$\phi_{a2} = \frac{P_{a2}}{P}\left[2N_m(P_{a1}+P_{a3})i_{ma} + N_b(P_{a1}-P_{a3})i_{sa1} - N_b(P_{a1}+P_{a3}+2P_{a4})i_{sa2}\right] \tag{6}$$

$$\phi_{a3} = \frac{-P_{a3}}{P}\left[2N_m(P_{a2}+P_{a4})i_{ma} - N_b(2P_{a1}+P_{a2}+P_{a4})i_{sa1} - N_b(P_{a2}-P_{a4})i_{sa2}\right] \tag{7}$$

$$\phi_{a4} = \frac{P_{a4}}{P}\left[2N_m(P_{a1}+P_{a3})i_{ma} + N_b(P_{a1}-P_{a3})i_{sa1} + N_b(P_{a1}+2P_{a2}+P_{a3})i_{sa2}\right] \tag{8}$$

where P is a sum of the permeances P_{a1}~P_{a4}.

Next, in order to calculate inductances, it is required to derive flux-linkages of each winding from the above equations. Consequently, the flux-linkage ψ_{ma} corresponding to motor winding current i_{ma} can be written from Fig. 5 as,

$$\psi_{ma} = (-\phi_{a1} + \phi_{a2} - \phi_{a3} + \phi_{a4})N_m. \tag{9}$$

Substituting the equations (5)~(8) into the equation (9) yields,

$$\begin{aligned}\psi_{ma} = {} & \frac{4N_m^2(P_{a1}+P_{a3})(P_{a2}+P_{a4})}{P} i_{ma} + \frac{2N_m N_b(P_{a1}-P_{a3})(P_{a2}+P_{a4})}{P} i_{sa1} \\ & - \frac{2N_m N_b(P_{a1}+P_{a3})(P_{a2}-P_{a4})}{P} i_{sa2}.\end{aligned} \tag{10}$$

Similarly, the flux-linkages ψ_{sa1} and ψ_{sa2} of the radial force windings can be written from Fig. 5 as,

$$\psi_{sa1} = (-\phi_{a1} + \phi_{a3})N_b \tag{11}$$

$$\psi_{sa2} = (-\phi_{a2} + \phi_{a4})N_b. \tag{12}$$

Substituting the equations (5)~(8) into the equations (11) and (12) yields,

$$\begin{aligned}\psi_{sa1} = {} & \frac{N_b^2\{P_{a1}(P_{a2}+2P_{a3}+P_{a4}) + P_{a3}(2P_{a1}+P_{a2}+P_{a4})\}}{P} i_{sa1} \\ & + \frac{2N_m N_b(P_{a1}-P_{a3})(P_{a2}+P_{a4})}{p} i_{ma} - \frac{N_b^2(P_{a1}-P_{a3})(P_{a2}-P_{a4})}{P} i_{sa2}\end{aligned} \tag{13}$$

$$\psi_{sa2} = \frac{N_b^2\{P_{a2}(P_{a1}+P_{a3}+2P_{a4})+P_{a4}(P_{a1}+2P_{a2}+P_{a3})\}}{P} i_{sa2} - \frac{2N_mN_b(P_{a1}+P_{a3})(P_{a2}-P_{a4})}{p} i_{ma} - \frac{N_b^2(P_{a1}-P_{a3})(P_{a2}-P_{a4})}{P} i_{sa1}. \quad (14)$$

Self-inductances and mutual inductances are given from coefficients of i_{ma}, i_{sa1} and i_{sa2} in the equations (10), (13), and (14).

$$L_{ma} = \frac{4N_m^2(P_{a1}+P_{a3})(P_{a2}+P_{a4})}{P} \quad (15)$$

$$L_{sa1} = \frac{N_b^2\{P_{a1}(P_{a2}+2P_{a3}+P_{a4})+P_{a3}(2P_{a1}+P_{a2}+P_{a4})\}}{P} \quad (16)$$

$$L_{sa2} = \frac{N_b^2\{P_{a2}(P_{a1}+P_{a3}+2P_{a4})+P_{a4}(P_{a1}+2P_{a2}+P_{a3})\}}{P} \quad (17)$$

$$M_{(ma,sa1)} = \frac{2N_mN_b(P_{a1}-P_{a3})(P_{a2}+P_{a4})}{p} \quad (18)$$

$$M_{(ma,sa2)} = -\frac{2N_mN_b(P_{a1}+P_{a3})(P_{a2}-P_{a4})}{p} \quad (19)$$

$$M_{(sa1,sa2)} = -\frac{N_b^2(P_{a1}-P_{a3})(P_{a2}-P_{a4})}{P} \quad (20)$$

where,

L_{ma}	the self-inductance of motor winding "ma".
L_{sa1}, L_{sa2}	the self-inductance of radial force windings 'sa1' and 'sa2'.
$M_{(ma,sa1)}$	the mutual inductance between motor winding 'ma' and radial force winding 'sa1'.
$M_{(ma,sa2)}$	the mutual inductance between motor winding 'ma' and radial force winding 'sa2'.
$M_{(sa1,sa2)}$	the mutual inductance between radial force winding 'sa1' and radial force winding 'sa2'.

B. Assumption and calculation of the permeance

Each permeance shown as P_{a1}~P_{a4} can be divided into three parts of permeances P_1~P_3 as shown in Fig. 6. P_2 and P_3 represent fringing path permeances. P_1 represents the permeance between poles. The following assumptions are considered in calculation.

(1) Magnetic saturation can be neglected.
(2) The rotor displacement is small enough compared with the air-gap length.
(3) Flux paths which do not link a rotor can be neglected.
(4) Flux paths between stator poles and rotor interpolar area can be neglected.

(5) Fringing fluxes only at the aligned position can be neglected, because an air-gap length is very short.

The assumed magnetic paths in the previous paper are made up of straight and circular lines. On the contrary, the assumed magnetic paths in this paper are composed of elliptical lines using a variable 'k'. In the previous paper, k is equal to 1. However, the variable k is dependent to the rotor rotational position and the air-gap length. The definitions of variables in Fig. 6 can be summarized as follows;

θ_a	rotor rotational position.
l_g	air-gap length.
r	radius of the rotor poles.
t	a position on a rotor circular surface.
dt	a derivative of t.
dP_2, dP_3	permeances of the infinitesimal width of the assumed magnetic path.

In Fig. 6, the fringing flux path has a width of dt and kdt at rotor and stator surfaces, respectively. k is a constant to determine the shape of ellipse. Thus, it is important to find the value of k. Fig. 7 shows flux paths obtained from FEM analysis. Fig. 8 shows an enlarged magnetic path at the pole edge. k can be calculated from each flux path in Fig. 8. FEM analysis is carried out with the air-gap lengths of 100μm, 220μm and 300μm to see the dependence of fringing fluxes to the air-gap length.

Fig. 9 shows the relationship between k and t derived from results of FEM analysis. Fig. 10 shows the relationship between k and t/l_g.

Regardless of l_g, k is found to be dependent to only t/l_g. Next, an average length of the flux path can be written with a simple approximation that an average of lengths of the semimajor and semiminor axes of the ellipse represent radius as,

$$l = \frac{\pi}{4}\left(t + l_g + kt\right) \tag{21}$$

where l is an average length of the magnetic path. This equation can be also written as,

$$\frac{l}{l_g} = \frac{\pi}{4}\left(1 + \frac{t}{l_g}\left(1 + k\right)\right). \tag{22}$$

Fig. 11 shows the relationship between l/l_g and t/l_g. It is seen that all the points are located in a line. The relationship between l/l_g and t/l_g can be approximated such that l/l_g and t/l_g have linear relationships. A simplified equation can be written as,

$$\frac{l}{l_g} = c\frac{t}{l_g} + \frac{\pi}{4} \tag{23}$$

where 'c' is a constant of 1.49. Substituting the equation (23) into the equation (22) yields,

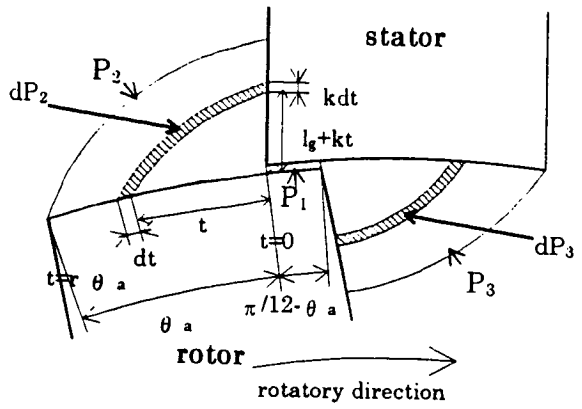

Fig.6 The assumed magnetic paths and permeances P_1~P_3.

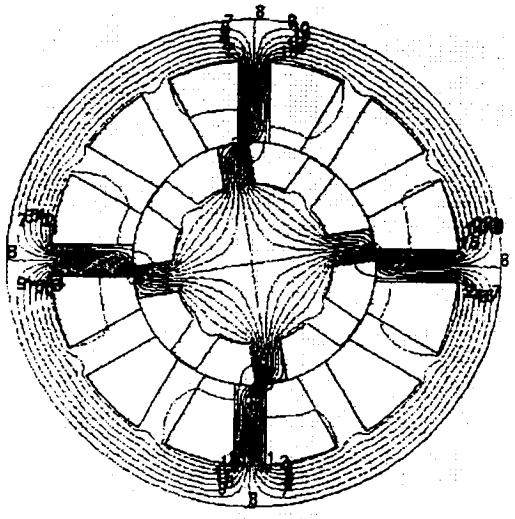

Fig.7 Flux distribution.

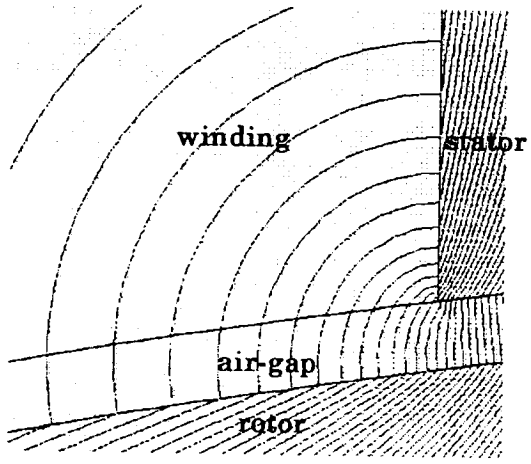

Fig.8 Enlarged flux paths.

$$k = \frac{4}{\pi}c - 1. \tag{24}$$

A cross section area of dP_2 can be approximated in the following equation (25).

$$s = \frac{h(dt + kdt)}{2} \tag{25}$$

where 's' is the cross section area of dP_2, 'h' is a stack length. Therefore, the relationship between $dP_2 \times l_g$ and t/l_g can be written as

$$dP_2 \times l_g = \frac{\mu_0 \times s}{l} \times l_g \tag{26}$$

where μ_0 is the permeability in the air. Substituting equations (22)~(25) into equation (26) yields,

$$dP_2 \times l_g = \frac{\delta \mu_0 hc}{\pi} \times \frac{1}{4c\dfrac{t}{l_g} + \pi} dt. \tag{27}$$

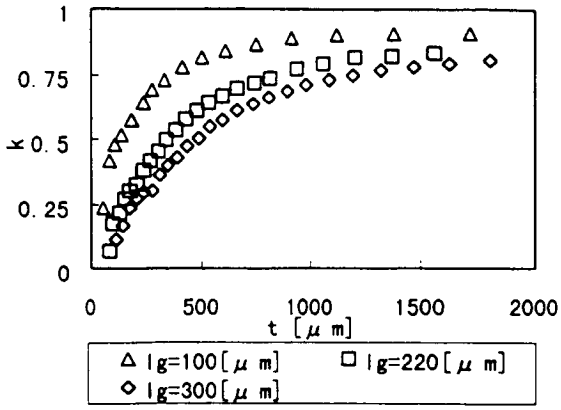

Fig.9 Relationship between k and t.

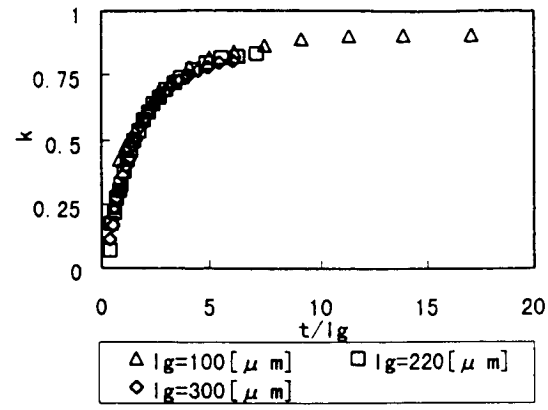

Fig.10 Relationship between k and t / l_g.

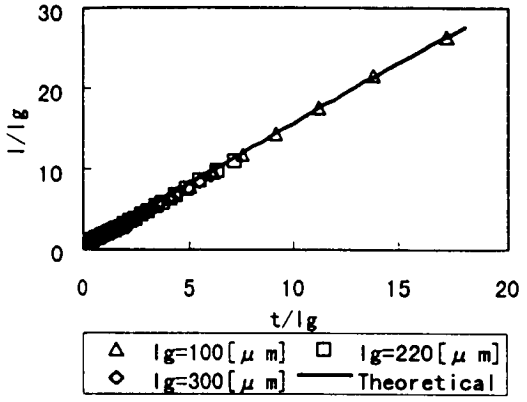

Fig.11 Relationship between l / l_g and t / l_g.

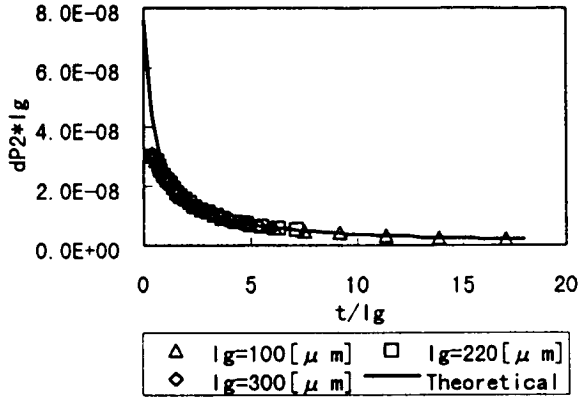

Fig.12 Relationship between $dP_2 \times l_g$ and t / l_g.

Fig. 12 shows the relationship between $dP_2 \times l_g$ and t/l_g. From Fig. 12, it is seen that the theoretical curve corresponds to the results of FEM analysis. Therefore, it is noted that the assumption of the equation (24) is effective. The equation (27) can be written as,

$$dP_2 = \frac{8\mu_0 hc}{\pi} \times \frac{1}{4ct + \pi l_g} dt . \tag{28}$$

The permeance P_1 of the air-gap between a rotor and stator poles can be derived as,

$$P_1 = \frac{\mu_0 hr\left(\frac{\pi}{12} - \theta_a\right)}{l_g} \tag{29}$$

where r is a radius of rotor poles. The permeance P_2 can be calculated from the equation (28) as

$$P_2 = \int_0^{r\theta_a} dP_2 . \tag{30}$$

Substituting the equation (28) into the equation (30) yields,

$$P_2 = \frac{2\mu_0 h}{\pi} ln\left(\frac{4cr\theta_a + \pi l_g}{\pi l_g}\right). \tag{31}$$

Similarly, the permeance P_3 can be derived considering symmetrical fringing flux paths as

$$P_3 = \frac{2\mu_0 h}{\pi} ln\left(\frac{4cr\theta_a + \pi l_g}{\pi l_g}\right). \tag{32}$$

The total permeances P_A is the sum of $P_1 \sim P_3$, thus,

$$P_A = P_1 + P_2 + P_3. \tag{33}$$

Therefore, from the equations (29) ~ (33),

$$P_A = \frac{\mu_0 hr\left(\frac{\pi}{12} - \theta_a\right)}{l_g} + \frac{4\mu_0 h}{\pi} ln\left(\frac{4cr\theta_a + \pi l_g}{\pi l_g}\right). \tag{34}$$

It is noted that P_{a1}, P_{a2}, P_{a3}, and P_{a4} are the equal to P_A if a rotor is positioned at the stator center.

C. Derivation of inductances

Substituting $l_0 \pm \alpha$ and $l_0 \pm \beta$ into the air-gap length l_g in the equation (34), the permeances $P_{a1} \sim P_{a4}$ are given, considering rotor radial displacements as,

$$P_{a1} = \frac{\mu_0 hr(\pi - 12\theta_a)(l_0 + \alpha)}{12{l_0}^2} + \frac{4\mu_0 h}{\pi} ln\left(\frac{4cr\theta_a(l_0 + \alpha) + \pi {l_0}^2}{\pi {l_0}^2}\right) \tag{35}$$

$$P_{a2} = \frac{\mu_0 hr(\pi - 12\theta_a)(l_0 - \beta)}{12{l_0}^2} + \frac{4\mu_0 h}{\pi} ln\left(\frac{4cr\theta_a(l_0 - \beta) + \pi {l_0}^2}{\pi {l_0}^2}\right) \tag{36}$$

$$P_{a3} = \frac{\mu_0 hr(\pi - 12\theta_a)(l_0 - \alpha)}{12{l_0}^2} + \frac{4\mu_0 h}{\pi} ln\left(\frac{4cr\theta_a(l_0 - \alpha) + \pi {l_0}^2}{\pi {l_0}^2}\right) \tag{37}$$

$$P_{a4} = \frac{\mu_0 hr(\pi - 12\theta_a)(l_0 + \beta)}{12{l_0}^2} + \frac{4\mu_0 h}{\pi} ln\left(\frac{4cr\theta_a(l_0 + \beta) + \pi {l_0}^2}{\pi {l_0}^2}\right) \tag{38}$$

where l_0 is the average air-gap length, α and β are the rotor displacements in the α- and β-axes, provided that l_0 is large enough to α and β. Substituting the equations (35)~(38) into the equations (15)~(20) yields,

$$L_{ma} = 2{N_m}^2\left(\frac{\mu_0 hr(\pi - 12\theta_a)}{6l_0} + \frac{8\mu_0 h}{\pi} ln\left(1 + \frac{4cr\theta_a}{\pi l_0}\right)\right) \tag{39}$$

$$L_{sa1} = {N_b}^2\left(\frac{\mu_0 hr(\pi - 12\theta_a)}{6l_0} + \frac{8\mu_0 h}{\pi} ln\left(1 + \frac{4cr\theta_a}{\pi l_0}\right)\right) \tag{40}$$

$$L_{sa2} = {N_b}^2\left(\frac{\mu_0 hr(\pi - 12\theta_a)}{6l_0} + \frac{8\mu_0 h}{\pi} ln\left(1 + \frac{4cr\theta_a}{\pi l_0}\right)\right) \tag{41}$$

$$M_{(ma,sa1)} = N_m N_b \left(\frac{\mu_0 hr(\pi - 12\theta_a)}{6{l_0}^2} \alpha + \frac{8\mu_0 h}{\pi} ln\left(\frac{4cr\theta_a(l_0 + \alpha) + \pi {l_0}^2}{4cr\theta_a l_0 + \pi {l_0}^2} \right) \right) \quad (42)$$

$$M_{(ma,sa2)} = N_m N_b \left(\frac{\mu_0 hr(\pi - 12\theta_a)}{6{l_0}^2} \beta + \frac{8\mu_0 h}{\pi} ln\left(\frac{4cr\theta_a(l_0 + \beta) + \pi {l_0}^2}{4cr\theta_a l_0 + \pi {l_0}^2} \right) \right) \quad (43)$$

$$M_{(sa1,sa2)} \approx 0 . \quad (44)$$

IV. DERIVATION OF RADIAL FORCES

A. Derivation of the theoretical equations of radial force

It is possible to construct a 3 x 3 inductance matrix from the derived self-inductances and mutual inductances in the equations (39)~(44). The 3 x 3 inductance matrix can be written as,

$$[L] = \begin{bmatrix} L_{ma} & M_{(ma,sa1)} & M_{(ma,sa2)} \\ M_{(ma,sa1)} & L_{sa1} & M_{(sa1,sa2)} \\ M_{(ma,sa2)} & M_{(sa1,sa2)} & L_{sa2} \end{bmatrix} \quad (45)$$

where, [L] is the 3 x 3 inductance matrix. The radial forces F_α and F_β can be derived from the derivatives of the stored magnetic energy with respect to displacements α and β, respectively. The stored magnetic energy can be written using the equation (45) as,

$$W_a = \frac{1}{2} \begin{bmatrix} i_{ma} & i_{sa1} & i_{sa2} \end{bmatrix} [L] \begin{bmatrix} i_{ma} \\ i_{sa1} \\ i_{sa2} \end{bmatrix} \quad (46)$$

where W_a is the stored magnetic energy. Thus, the radial forces F_α and F_β are given, substituting the equations (39)~(44) into the equation (46), yields,

$$F_\alpha = \frac{\partial W_a}{\partial \alpha} = N_m N_b \left(\frac{\mu_0 hr(\pi - 12\theta_a)}{6{l_0}^2} + \frac{32\mu_0 hrc\theta_a}{\pi\left(4rc\theta_a(l_0 + \alpha) + \pi {l_0}^2\right)} \right) i_{ma} i_{sa1} \quad (47)$$

$$F_\beta = \frac{\partial W_a}{\partial \beta} = N_m N_b \left(\frac{\mu_0 hr(\pi - 12\theta_a)}{6{l_0}^2} + \frac{32\mu_0 hrc\theta_a}{\pi\left(4rc\theta_a(l_0 + \beta) + \pi {l_0}^2\right)} \right) i_{ma} i_{sa2} . \quad (48)$$

The following points are clear from the equations (47) and (48).

(1) The radial forces F_α and F_β are directly proportional to the products of motor winding current i_{ma} and radial force winding currents i_{sa1} or i_{sa2}. Therefore, the radial forces can be controlled by radial force winding current. Let us define a radial force constant K_f as $F_\alpha / (i_{ma} i_{sa1})$ and $F_\beta / (i_{ma} i_{sa2})$.

(2) The radial force constant K_f is dependent on rotor rotational position θ_a. The first term in the parentheses originates from the permeance between rotor and stator poles. Thus, the first term is dominant, and decreases linearly as θ_a increases. At $\theta_a = \pi/12$, the first term becomes zero. Note that the equations (47) and (48) are valid only $0 \leq \theta_a \leq \pi/12$ (15deg). If $\theta_a > \pi/12$, then the first term is zero. In this condition, rotor poles are not facing stator poles. The second term corresponding to fringing paths now plays an important role.

(3) In low speed operations, motor current is usually injected during $0 \leq \theta_a \leq$ 15deg to produce torque efficiently. Thus, it is important to examine K_f in this condition, especially θ_a is around 15deg.

B. The measurement and the examination of the radial forces

A test machine was built and the magnetic suspension realized with DC current in A-phase windings. In this situation, weights are hung to apply radial force as shown in Fig. 13. An average current in the radial force windings is measured. In every rotational position, weights are increased and then decreased while the average current is measured. The hysteresis influence is small enough to obtain relationships between radial force and radial force winding current. Then, K_f is obtained from the Least-Square Error method. A ratio of lengths from the fulcrum to the mechanical force application point and the central point of the active area is 2.316:1. This ratio is considered.

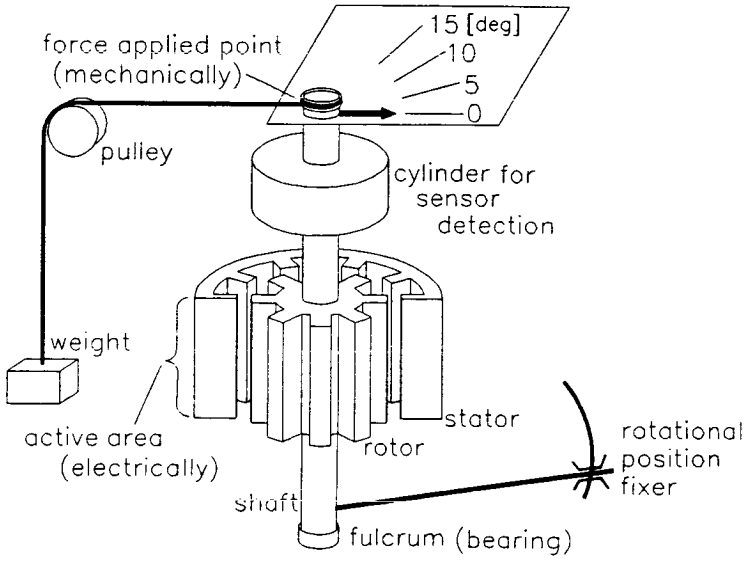

Fig. 13 A model of the experiment.

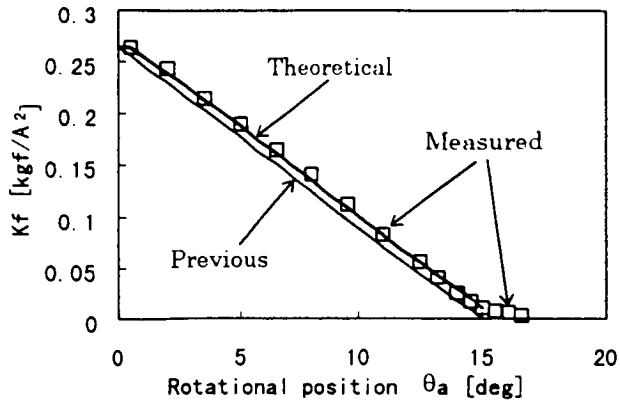

Fig.14 Relationship between K_f and θ_a.

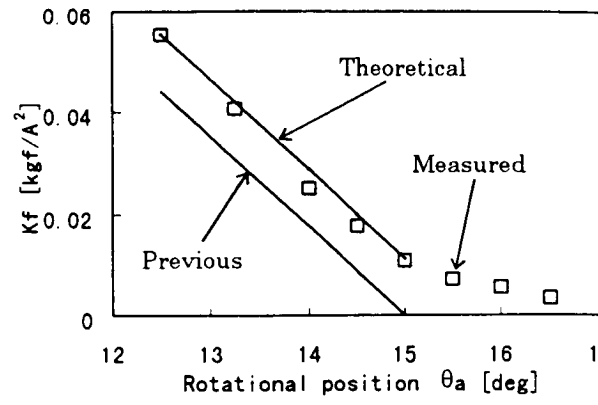

Fig.15 Magnification of unaligned position.

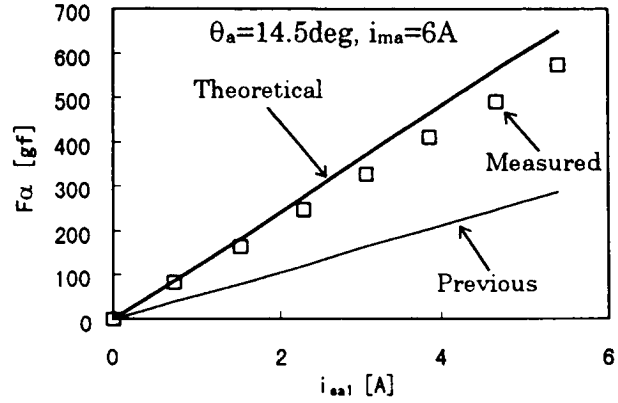

Fig.16 Relationship between F_α and i_{sa1}.

Fig. 14 shows the relationship between the radial force constant K_f and the rotor rotational position θ_a. Fig. 15 shows the magnification in a range of θ_a = 12.5~15deg. Fig. 16 shows the relationship between the radial forces F_α and the radial force winding current i_{sa1} at θ_a = 14.5deg. The theoretical value in the previous paper [12] is also drawn. This value is originated from only the first term in the parentheses of the equations (47) and (48). It is seen that the proposed calculation is especially effective in a range of θ_a = 13~15deg. As the accurate inverse function of K_f is required in controller to keep constant loop gain, while a test machine is rotating, accurate theoretical estimation is important. The second term in the parentheses is found to be effective to derive the radial force constant, especially at unaligned positions.

V. CONCLUSIONS

In this paper, the theoretical equations of radial forces are derived with a close examination of flux distribution. Based on results of FEM analysis, simple mathematical equations are proposed to express fringing fluxes. Relationships between radial force and current around unaligned positions are derived with the fringing effects. It is stated that the derived equations are especially effective at unaligned positions. These relationships are confirmed in experiments.

REFERENCES

[1] Ichikawa O., Michioka C., Fukao T., and Chiba A., "A Decoupling Control Method of Radial Rotor Position in Synchronous Reluctance Type Bearingless Motors", IPEC-Yokohama'95, pp.347-351, 1995.

[2] A. Chiba, R. Furuichi, Y. Aikawa, K. Shimada, Y. Takamoto, and T. Fukao, "A Stable Operation of Induction Type Bearingless Motors under Loaded Conditions", IEEE Trans. of Industry Applications, Vol.33, No.44, pp.919-924, 1997.

[3] A. Chiba, R. Miyatake, S. Hara, and T. Fukao, "Transfer Characteristics of Radial Force of Induction Type Bearingless Motors with Four-Pole Rotor Circuits", Fifth International Symposium on Magnetic Bearings,Kanazawa, pp.319-325, 1996.

[4] R. Schöb, "Applications of the Lateral-Force-Motor (LFM)", IPEC-Yokohama'95, pp.358-363, 1995.

[5] M. Ooshima, A. Chiba, T. Fukao, and M. Azizur Rahman, "Design and Analysis of Permanent Magnet-Type Bearingless Motors", IEEE Transactions., Indus. Electr., Vol.IE-43, No.2, pp.292-299, 1996.

[6] T. Ohishi, Y. Okada, and S. Miyamoto, "Levitation Control of IPM Type Rotating Motor", Fifth International Symposium on Magnetic Bearings, Kanazawa, pp.327-332, 1996.

[7] Eike Richter and Caio Frreira, "Performance Evaluation of a 250kW Switched Reluctance Starter Generator", IEEE IAS'95, pp.434-440, 1995.

[8] Kaushik R., "Propulsion System Issues in Electric and Hybrid Vehicle Applications", IPEC-Yokohama'95, pp.93-98, 1995.

[9] T. Higuchi, H. Kawakatsu, and T. Iwasawa, "A study on magnetic suspension of switched reluctance motor", IEE of Japan, Annual Meeting Record 684, pp.(6-122)-(6-123), 1989 (in Japanese).

[10] Mark A., James P. F., Eike Richter, and Kiyoung Chung, "Integrated magnetic bearing / switched reluctance machine", U.S. Patent 5,424,595, 1994.

[11] T. Higuchi and T. Komori, "z-θ positioning contactless actuator", Proc. of 6th Robot Institute of Japan, pp.281-282, 1988 (in Japanese).

[12] K. Shimada, M. Takemoto, A. Chiba, and T. Fukao, "Radial Forces in Switched Reluctance Type Bearingless Motors", The 9th Symposium on Electromagnetics and Dynamics, pp.547-552, 1997 (in Japanese).